

# Atmospheric wind biases: A challenge for simulating the Arctic Ocean in coupled models?

Claudia Hinrichs<sup>1</sup>, Qiang Wang<sup>2</sup>, Nikolay V. Koldunov<sup>2</sup>, Longjiang Mu<sup>2</sup>, Tido Semmler<sup>3</sup>, Dmitry Sidorenko<sup>2</sup>, and Thomas Jung<sup>4</sup>

<sup>1</sup>Alfred Wegener Institute, Helmholtz Centre for Polar and Marine Research

<sup>2</sup>Alfred Wegener Institute for Polar and Marine Research

<sup>3</sup>Alfred Wegener Institute Helmholtz Centre for Polar and Marine Research

<sup>4</sup>AWI

November 23, 2022

## Abstract

Many state-of-the-art climate models do not simulate the Atlantic Water (AW) layer in the Arctic Ocean realistically enough to address the question of future Arctic Atlantification and its associated feedback. Biases concerning the AW layer are commonly related to insufficient resolution and exaggerated mixing in the ocean component as well as unrealistic Atlantic-Arctic Ocean exchange. Based on sensitivity experiments with FESOM1.4, the ocean-sea ice component of the global climate model AWI-CM1, we show that even if all impediments for simulating AW realistically are addressed in the ocean model, new biases in the AW layer develop after coupling to an atmosphere model. By replacing the wind forcing over the Arctic with winds from a coupled simulation we show that a common bias in the atmospheric sea level pressure (SLP) gradient and its associated wind bias lead to differences in surface stress and Ekman transport. Fresh surface water gets redistributed leading to changes in steric height distribution. Those changes lead to a strengthening of the anticyclonic surface circulation in the Canadian Basin, so that the deep counterflow carrying warm AW gets reversed and a warm bias in the Canadian Basin develops. An underestimation of sea ice concentration can significantly amplify the induced ocean biases. The SLP and anticyclonic wind bias in the Nordic Seas weaken the cyclonic circulation leading to reduced AW transport into the Arctic Ocean through Fram Strait but increased AW transport through the Barents Sea Opening. These effects together lead to a cold bias in the Eurasian Basin.



**18 Abstract**

19 Many state-of-the-art climate models do not simulate the Atlantic Water (AW) layer in  
20 the Arctic Ocean realistically enough to address the question of future Arctic Atlantification and  
21 its associated feedback. Biases concerning the AW layer are commonly related to insufficient  
22 resolution and exaggerated mixing in the ocean component as well as unrealistic Atlantic-Arctic  
23 Ocean exchange. Based on sensitivity experiments with FESOM1.4, the ocean-sea ice  
24 component of the global climate model AWI-CM1, we show that even if all impediments for  
25 simulating AW realistically are addressed in the ocean model, new biases in the AW layer  
26 develop after coupling to an atmosphere model. By replacing the wind forcing over the Arctic  
27 with winds from a coupled simulation we show that a common bias in the atmospheric sea level  
28 pressure (SLP) gradient and its associated wind bias lead to differences in surface stress and  
29 Ekman transport. Fresh surface water gets redistributed leading to changes in steric height  
30 distribution. Those changes lead to a strengthening of the anticyclonic surface circulation in the  
31 Canadian Basin, so that the deep counterflow carrying warm AW gets reversed and a warm bias  
32 in the Canadian Basin develops. An underestimation of sea ice concentration can significantly  
33 amplify the induced ocean biases. The SLP and anticyclonic wind bias in the Nordic Seas  
34 weaken the cyclonic circulation leading to reduced AW transport into the Arctic Ocean through  
35 Fram Strait but increased AW transport through the Barents Sea Opening. These effects together  
36 lead to a cold bias in the Eurasian Basin.

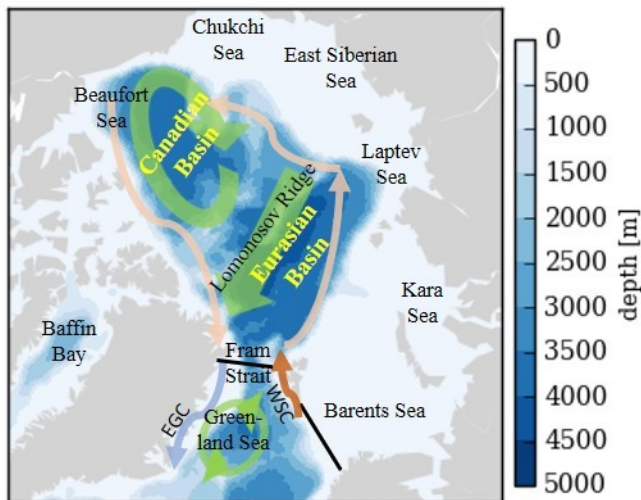
**37 Plain Language Summary**

38 Coupled global climate models are used to predict anthropogenic climate change along  
39 with its impacts. The Arctic has experienced amplified warming in the recent decades compared  
40 to global mean warming and therefore is one region of intense climate research. In this context  
41 Atlantification of the Arctic has become a high priority topic. Atlantification, describes the  
42 increasing impact of oceanic heat in the form of Atlantic-origin water within the Arctic Ocean  
43 and on the sea ice cover. In climate models, the direction and strength of simulated Atlantic  
44 Water (AW) circulation around the Arctic Ocean is known to be sensitive to ocean grid  
45 resolution, parametrization, boundary and surface forcing or a combination thereof. Here we  
46 show that biases in the atmospheric component of climate models can interrupt and even reverse

47 the simulated AW circulation at depth. Such biases can be further amplified by negative bias in  
 48 simulated sea ice. The impact pathways of the wind biases are investigated in this study.

## 49 1 Introduction

50 The Arctic is one of the fastest changing regions in the world (Serreze et al. 2009;  
 51 Serreze and Barry 2011) and hence has attracted an increasing amount of scientific work. Global  
 52 climate models are used to predict changes in the climate system, including the Arctic, that may  
 53 occur in a warming world and to understand climate dynamics and associated feedback. There is  
 54 an ongoing effort to improve the representation of key processes in contemporary climate models  
 55 in general and in the Arctic specifically, with the ultimate aim to increase predictive capacity  
 56 (Jung et al. 2016). One of the processes of particular interest is the oceanic heat transport from  
 57 the North Atlantic into the Arctic Ocean in the form of Atlantic Water (AW) inflow and the  
 58 subsequent AW circulation and heat distribution within the Arctic Basin and how it will change  
 59 in the future.



60

61 **Figure 1.** Map of the Arctic Ocean. The two main basins (Canadian and Eurasian Basin) divided by the Lomonosov  
 62 Ridge, the shelf seas and neighboring seas are depicted. A schematic view of the dominant features of the Arctic  
 63 Ocean circulation shows the anticyclonic Beaufort Gyre System, the Transpolar Drift System in green and the  
 64 subsurface cyclonic flow of AW around the Arctic Basin is sketched in pink. South of Fram Strait, the Greenland  
 65 Sea Gyre (GSG) is sketched in green, and the West Spitsbergen Current (WSP, orange) and the East Greenland  
 66 Current (EGC, lightblue) are shown. Sections where transports through Fram Strait and the southern Barents Sea  
 67 Opening are computed are shown in black.

68 Over the last few decades, a warming trend in the AW layer has been observed at Fram  
 69 Strait and in the Arctic Ocean (Polyakov et al. 2005; Dmitrenko et al. 2008; Beszczynska-Möller  
 70 et al. 2012; Polyakov et al. 2013). This warming trend of the AW layer together with weaker

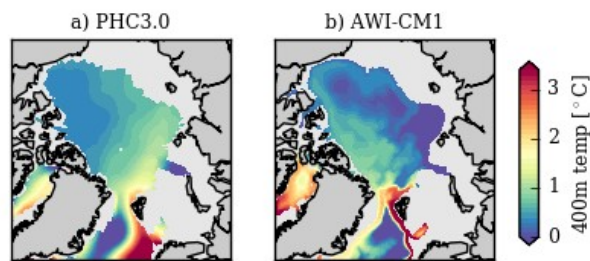
71 stratification in the upper ocean has been termed *Atlantification* by Polyakov et al. (2017). This  
72 phenomenon has been identified as critical in a warming Arctic. In the Barents Sea,  
73 Atlantification leads to increased bottom melt of sea ice, more open water area, increased surface  
74 temperatures and lower albedo (Koenigk and Brodeau 2014; Barton et al. 2018). In the Eurasian  
75 Basin (EB), Atlantification is associated with weakened stratification, increased vertical mixing,  
76 and increased sea-ice decline (Polyakov et al. 2017; Ivanov et al. 2018; Polyakov et al. 2020).  
77 The sea ice decrease, caused by Atlantification and its associated feedback, contributes to  
78 amplified climate change in the Arctic. Sea ice decline also affects the AW layer in the Arctic  
79 Ocean. A model study by (Itkin et al. 2014), for example, suggests that thinner, more mobile sea  
80 ice in the central Arctic weakens the cyclonic circulation of AW. Another study by Wang et al.  
81 (2020) shows that the Arctic sea ice decline has strengthened the AW heat influx through Fram  
82 Strait by impacting the ocean circulation in the Nordic Seas. There is also an ongoing debate that  
83 Arctic changes, and especially sea ice cover in the Barents Sea, could possibly have a large  
84 influence on the lower latitude ocean and climate (e.g. Vihma 2014; Wallace et al. 2014; Cohen  
85 et al. 2020).

86 In order to understand and predict the evolution of this complex system coupled climate  
87 models constrained by observations are an important tool. However, the degree to which we can  
88 trust climate model predictions of the future role of Atlantification in Arctic climate change,  
89 hinges on their ability to simulate the present-day AW inflow and circulation within the Arctic  
90 Ocean realistically.

91 The circulation of the Arctic Ocean can be described as a two-layer system (e.g. Aagaard  
92 1989; for a recent, comprehensive review of Arctic Ocean circulation dynamics see Timmermans  
93 and Marshall 2020). The large-scale ocean surface circulation is anticyclonic, driven by the  
94 dominating wind systems centered over the Beaufort Gyre and the Transpolar Drift Zone. Below  
95 the surface layer the flow at intermediate depth is largely concentrated in narrow boundary  
96 currents along the steep slopes of the Eurasian and Canadian Basins (see Figure 1). These  
97 boundary currents flow in cyclonic direction around the deep Arctic Basin, opposite to the upper  
98 ocean drift. Relatively warm and salty AW circulates the Arctic in this cyclonic boundary current  
99 (Rudels et al. 1999; Woodgate et al. 2001; Karcher et al. 2007; Spall 2013) at a mean depth of  
100 around 400m. The strength and direction of this Arctic circumpolar boundary current (ACBC)

101 determines the spatial distribution and storage of heat in the Arctic Ocean at this intermediate  
 102 depth.

103 With this in mind, we compared the 400 m temperature layer in the Alfred Wegener  
 104 Institute coupled climate model AWI-CM1 (Sidorenko et al. 2015; Rackow et al. 2016; Semmler  
 105 et al. 2020) to the PHC3.0 climatology (Steele et al. 2001) (Figure 2). The horizontal temperature  
 106 distribution can serve as a proxy for AW circulation in the Arctic Ocean. For the AWI-CM1  
 107 simulation, the comparison reveals an unrealistic distribution of AW: Warm AW that enters  
 108 through Fram Strait does not follow the Arctic's deep basin slope cyclonically; it rather gets  
 109 diverted westward towards the Canadian Basin. The result is a cold bias in the eastern Eurasian  
 110 Basin and a warm bias in the Canadian Basin that is reminiscent of an anticyclonic circulation  
 111 pattern.



112

113 **Figure 2.** 400 m temperature from PHC3.0 climatology (a) and a 10-year average from a coupled AWI-CM1.1  
 114 simulation (b). Shown here is a simulation on an ocean grid with 25km resolution north of 50°N and T63  
 115 atmospheric resolution. A similar bias pattern is also evident in runs with higher ocean or atmosphere resolution.

116 This finding came somewhat as a surprise, after standalone simulations with AWI-CM1's  
 117 ocean-sea ice component FESOM1.4 had shown a very realistic temperature distribution and a  
 118 cyclonic circumpolar boundary current for horizontal resolutions of 25 km and 4.5 km in Arctic  
 119 (Wang et al. 2018).

120 It is worth stressing that not only AWI-CM1 is deficient in simulating the propagation of  
 121 AW around the Arctic, as revealed by some recent studies. Shu et al. (2019), for example,  
 122 evaluated a number of CMIP5 models and found that 9 out of 41 participating models did not  
 123 simulate a well-defined AW layer at all. The multi-model mean (MMM) AW layer derived from  
 124 the other 32 models was too thick and too deep. Furthermore, they found that the interannual  
 125 variability in AW temperature was much weaker than observed; and none of the models  
 126 simulated the observed warming trend of the recent decades. A follow-up study of 23 CMIP6  
 127 models by (Khosravi et al., submitted) shows that the AW layer is still too deep and too thick in

128 most models and the MMM, thus suggesting that the representation of the Arctic Ocean  
129 hydrography did not visibly improve from CMIP5 to CMIP6. Preceding CMIP6, the problem of  
130 incorrect AW simulation was also recognized in standalone ocean models in the CORE-II model  
131 intercomparison study (Ilicak et al. 2016). Suggested solutions for the AW problem have been  
132 focusing on improving the ocean-sea ice model and include moving to higher-order advections  
133 schemes (Maqueda and Holloway 2006; Holloway et al. 2007), using eddy–topography  
134 interaction parameterization (“Neptune parametrization”) (e.g. Golubeva and Platov 2007;  
135 Holloway and Wang 2009; Nazarenko et al. 1998), tuning vertical mixing (Zhang and Steele  
136 2007) and increasing horizontal resolution (Wang et al. 2018). We find for AWI-CM1 that  
137 additional challenges can arise when a well-tuned (with respect to AW in the Arctic Ocean)  
138 ocean-sea ice model, here FESOM 1.4 (Wang et al. 2014; Danilov et al. 2015), is coupled to an  
139 atmospheric model, in this case ECHAM6.3 (Stevens et al. 2013), to form a coupled climate  
140 model.

141         In this paper we aim to understand the processes causing the deterioration of the AW  
142 layer in AWI-CM1. If the standalone version of an ocean-sea ice model can successfully  
143 replicate the two-layer circulation in the Arctic Ocean, but coupling leads to a perturbed AW  
144 circulation, then the reason must lie in the changes in ocean surface forcing after coupling with  
145 the atmosphere model. Our investigations narrowed the potential origins of these biases down to  
146 a large-scale bias in sea level pressure and the associated wind field and a negative bias in the sea  
147 ice cover in the coupled model, both have an impact on the surface stress imparted on the ocean.  
148 We conducted sensitivity experiments with our standalone ocean-sea ice model, to analyze the  
149 influence of biased wind and biased sea ice cover over the Arctic .

## 150 **2 Model set-up and sensitivity experiments**

### 151 2.1 FESOM1.4 Model Configuration

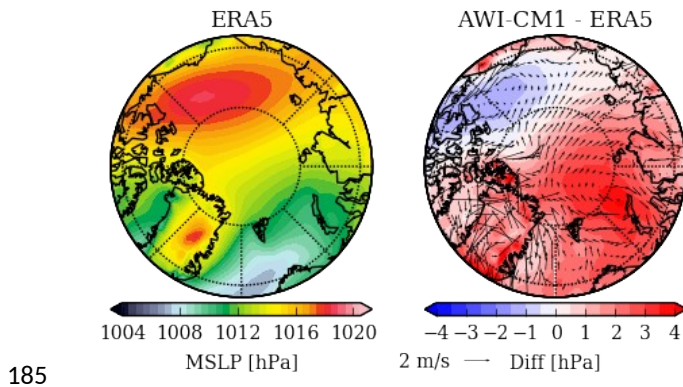
152 To study the effect of atmosphere forcing and sea ice concentration on the AW circulation  
153 we use the **Finite Element Sea ice-Ocean Model** FESOM1.4 (Wang et al. 2014; Danilov et al.  
154 2015) in standalone mode. FESOM1.4 is the ocean-sea ice component of the Alfred-Wegener-  
155 Institute’s climate model version 1 (AWI-CM1) which is coupled to ECHAM6.3 (Stevens et al.  
156 2013). The global performance of AWI-CM1 has been evaluated in Sidorenko et al. (2015) and  
157 Rackow et al. (2016), and for the AWI-CM1 CMIP6 contribution by Semmler et al. (2020).

158 FESOM employs unstructured grids which allow for increased grid resolution in an area of  
159 interest (e.g., the Arctic) while keeping the resolution coarser elsewhere. This, along with  
160 excellent scalability characteristics (Koldunov et al. 2019), makes longer, global simulations  
161 affordable. The problem with incorrect AW circulation and distribution in the coupled set-up is  
162 almost independent of ocean and atmosphere resolution (at least for AWI-CM1). Therefore, the  
163 sensitivity experiments are run on the ‘baseline’ ocean grid which was developed for the  
164 participation in the CORE-II Model Intercomparison Study (Griffies et al. 2009; Wang et al.  
165 2016a, 2016b; Ilıcak et al. 2016). We will compare our sensitivity experiments to a coupled  
166 historical simulation run on the same ocean grid and an atmospheric resolution of T63 in the  
167 horizontal and 47 vertical levels. The ocean grid has a nominal resolution of 1° globally;  
168 however, the resolution has been refined to about 25 km north of 50°N and to 1/3° at the equator,  
169 and it is also refined moderately along the coasts. In the CORE-II model intercomparison study  
170 the ocean circulation itself is not evaluated, but the 400 m temperature layer is shown for each  
171 model, and for FESOM1.4 the temperature distribution indicates a realistic pathway of AW into  
172 and around the Arctic (Ilıcak et al. 2016). A more detailed evaluation of Atlantic Water core  
173 temperature (AWCT) and Atlantic Water core depth (AWCD) in simulations on this baseline grid  
174 show a temperature pattern indicating the correct circulation direction (Wang et al. 2018).

175 The comparison of AWI-CM1 coupled simulations to atmospheric reanalysis data and sea ice  
176 satellite observations revealed biases in the wind field over the Arctic and in the sea ice cover  
177 that were considered possible candidates for causing biases in the ocean of the coupled setup.  
178 These biases are briefly described in the following.

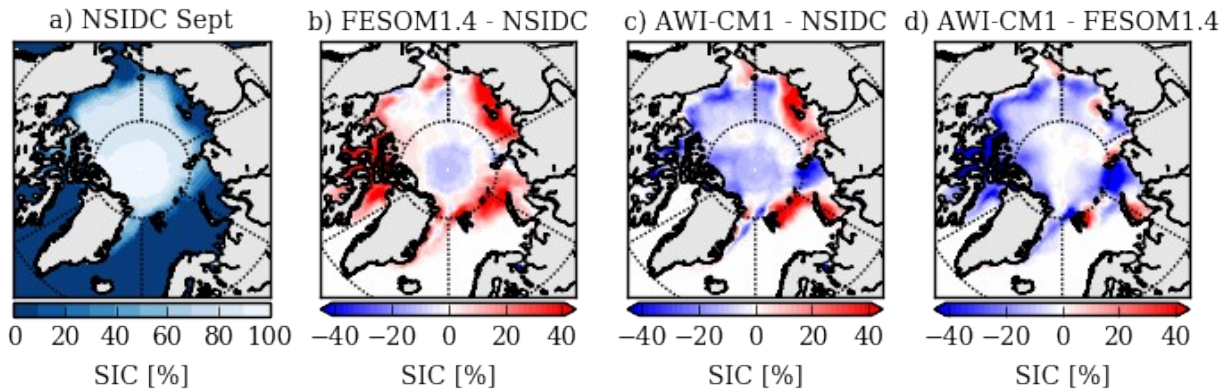
## 179 2.2 Coupled model bias in mean sea level pressure and sea ice

180 The comparison of mean sea level pressure (SLP) to the ERA5 reanalysis dataset  
 181 (Hersbach et al. 2020) shows that AWI-CM1 has a bias over the central Arctic which has a dipole  
 182 pattern: erroneously low SLP is found over the Canada Basin, whereas SLP is biased high over  
 183 the Eurasian Basin and Barents and Kara Seas (Figure 3). The reduced pressure gradient is  
 184 associated with a shift of the Beaufort High towards the Eurasian Arctic.



186 **Figure 3.** Mean annual sea level pressure (MSLP, [hPa]) 1980-1989 in ERA5 (left), MSLP bias [hPa] and associated  
 187 wind bias in AWI-CM1 (right).

188 This dipole bias pattern is not unique to AWI-CM1. The coupled climate model MPI-ESM  
 189 (Müller et al. 2018) which also uses ECHAM6.3 but a different ocean-sea ice model shows the  
 190 same bias in pattern and magnitude (not shown). A similar SLP bias pattern also dominated the  
 191 model mean of other atmospheric and coupled models not including ECHAM and it has been  
 192 attributed to the truncation of the North Atlantic storm track in atmosphere models (Walsh et al.  
 193 2002).



194  
 195 **Figure 4.** Mean September sea ice concentration (SIC, [%]) 1980-1989 from NSIDC (a), difference in SIC between  
 196 FESOM1.4 and NSIDC (b), difference in SIC between AWI-CM1 and NSIDC (c), and difference in SIC between  
 197 AWI-CM1 and FESOM1.4 (d)

198 The comparison of average September sea ice concentration from the coupled simulation to a  
 199 standalone ocean ice model simulation and to satellite observations (NSIDC, Cavalieri (1996))  
 200 shows that AWI-CM1 generally simulates less sea ice than observed, except in some shelf  
 201 regions including the north-eastern Barents Sea and the East Siberian Sea, and less sea ice than  
 202 FESOM1.4 in forced (CORE-II forcing) mode (Figure 4). Underestimation of sea ice  
 203 concentration in AWI-CM1 is also found in other seasons (not shown).

### 204 2.3 Sensitivity Experiments

205 Three sensitivity experiments have been devised to determine the impact of the wind bias  
 206 and the bias in sea ice cover (separately and together) on AW circulation at depth (Table 1). A  
 207 control simulation and the sensitivity experiments were started in 1958 from EN4 climatology  
 208 (Good et al. 2013) and run with CORE-II forcing (Large and Yeager 2009) for 32 years until  
 209 1990. In sensitivity experiment 1 (WIND) the 6-hourly CORE-II wind forcing north of 67°N, the  
 210 Arctic Circle, was replaced with wind from an AWI-CM1 historical simulation run on the same  
 211 ocean grid that also started in 1958 from EN4. The 6-hourly AWI-CM1 wind output was  
 212 interpolated onto the CORE-II forcing grid. In sensitivity experiment 2 (ALBEDO), the ice and  
 213 snow albedos are lowered to a degree where the sea ice cover is reduced to values similar to the  
 214 ones found in the coupled simulation. In sensitivity experiment 3 (WIND+ALB) both changes  
 215 were applied together.

216 **Table 1.** Overview sensitivity experiments

	<b>CTL</b>	<b>WIND</b>	<b>ALBEDO</b>	<b>WIND+ALB</b>
Wind Forcing	CORE2 forcing	CORE2 forcing, except wind forcing north of 67°N replaced with wind from coupled simulation	CORE2 forcing	CORE2 forcing, except wind forcing north of 67°N replaced with wind from coupled simulation
Albedo Parameters	default	default	reduced	reduced

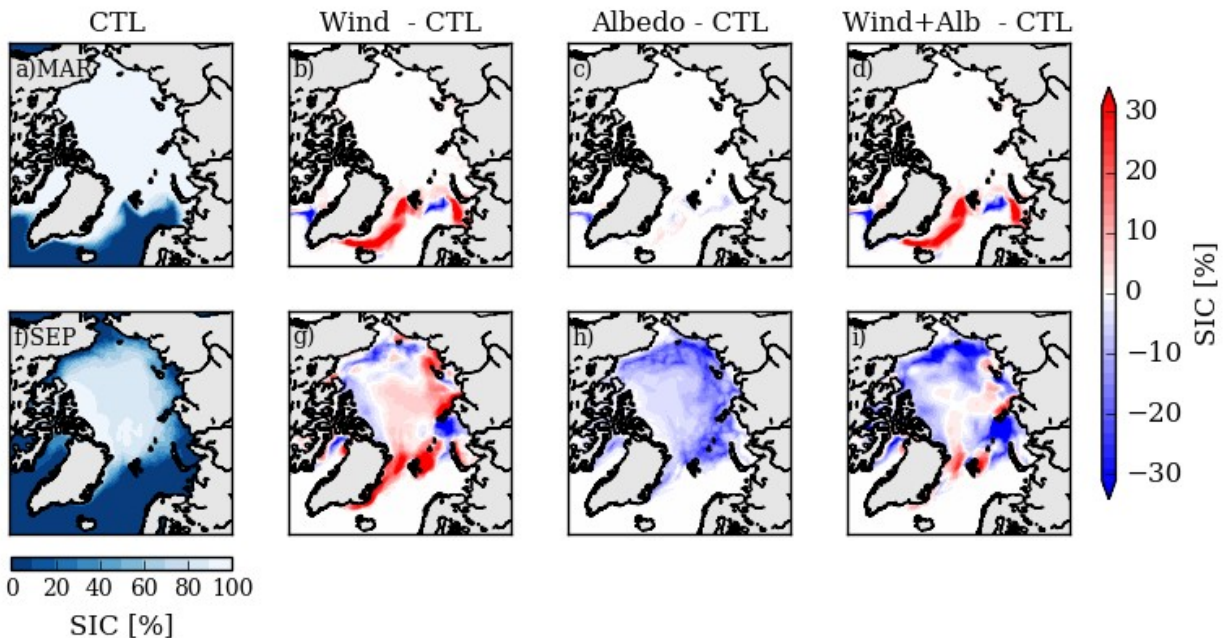
217 In all four experiments the drag coefficients for the wind stress computation over ice and  
218 over water were adapted to follow the stress computation in the atmospheric component of AWI-  
219 CM1, ECHAM6.3, as closely as possible. The neutral drag coefficient over ice  $Cd_{n,i}$  is set to  
220  $1.89e-3$ , the same value as in ECHAM6.3. The neutral drag coefficient over water  $Cd_{n,w}$  is  
221 usually dependent on wind speed and computed using a bulk formula. In ECHAM6.3 it is  
222 computed using the Charnock equation (Charnock 1955). For our experiments using FESOM1.4  
223 the neutral drag coefficient over water  $Cd_{n,w}$  was set to be a constant value,  $1.285e-3$ . This value  
224 represents the mean value of applying the Charnock relation to the most common wind speeds  
225 values over the Arctic, which are between 1 m/s and 8 m/s .

226 The results from the sensitivity experiments are described in the following section.

### 227 **3 Results Sensitivity Experiments**

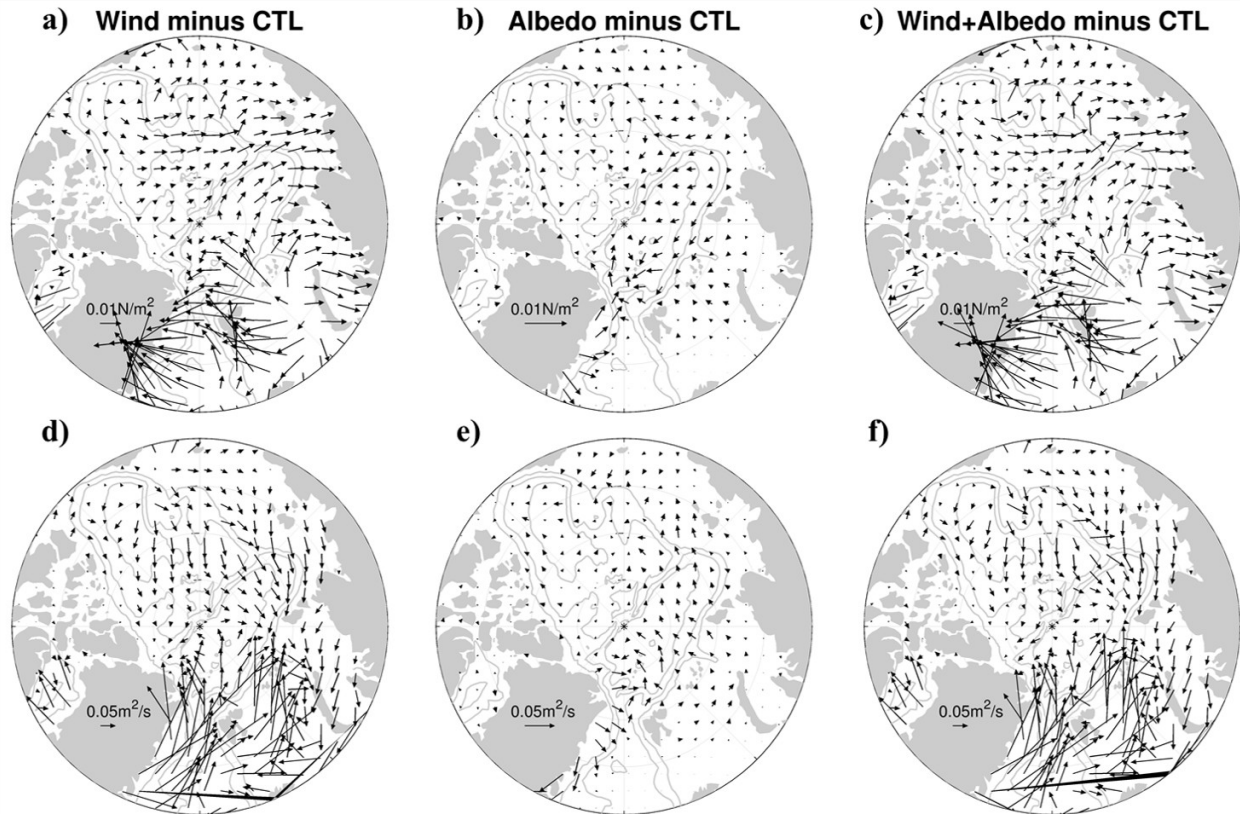
228 First, the effect of exchanging the wind forcing and lowering the albedo on mean sea ice  
229 concentration in March and September is assessed (Figure. 5). In winter, replacing the wind  
230 forcing over the Arctic circle with wind from the coupled model results in increased sea ice  
231 concentration along the ice edge in the Greenland Sea and eastern Barents Sea. More spatially  
232 confined reductions in sea ice concentration can be seen in Davis Strait and in the central Barents  
233 Sea. In March, the reduced albedo has almost no effect on the sea ice extent, only on the sea ice  
234 thickness (not shown). Therefore, in March, the combined effect of a changed wind forcing and a  
235 reduced albedo is governed by the wind replacement in terms of sea ice concentration.  
236 In September, the wind replacement leads to decreased sea ice concentration north of the  
237 Canadian Archipelago, in the Beaufort, Chukchi, East Siberian and Kara Seas and increased sea

238 ice concentration in the Laptev Sea, in the central Arctic along the transpolar drift route and in  
 239 the northern Barents Sea and along eastern Greenland. Reduced albedo leads to a decrease in sea  
 240 ice concentration everywhere. When wind replacement and albedo reduction are combined in  
 241 experiment WIND+ALB, the sea ice concentration is mostly lower than in the control simulation  
 242 except along the transpolar drift route and east of Svalbard, which is associated with the impact  
 243 of winds. The significance of the impacts of changing winds and albedo on sea ice in other  
 244 seasons lies between winter and summer.



245 **Figure 5.** Differences in sea ice concentration (SIC, [%]) for March (top) and September (bottom) to control  
 246 simulation  
 247

248 Next, the effect of the replaced wind and the albedo reduction on ocean surface  
 249 conditions was investigated. The difference in surface stress between the sensitivity experiment  
 250 with replaced wind forcing and the control run in the central Arctic (Figure 6a) is generally  
 251 acting from the Canadian Arctic Archipelago towards the Siberian side. In the Barents Sea and  
 252 the Nordic Seas, the difference in surface stress is directed westward. The surface stress  
 253 difference due to reduced sea ice cover is relatively small, showing a westward component in the  
 254 Eurasian Basin (Figure 6b). The differences due to the replaced wind dominate in sensitivity  
 255 experiment WIND+ALB (Figure 6c).



256

257 **Figure 6.** Ocean surface stress difference [ $\text{N}/\text{m}^2$ ] (a-c) and Ekman transport difference [ $\text{m}^2/\text{s}$ ] (d-f) for the three  
 258 sensitivity experiments relative to the control run. Note that the scale for the experiment ALBEDO is doubled.

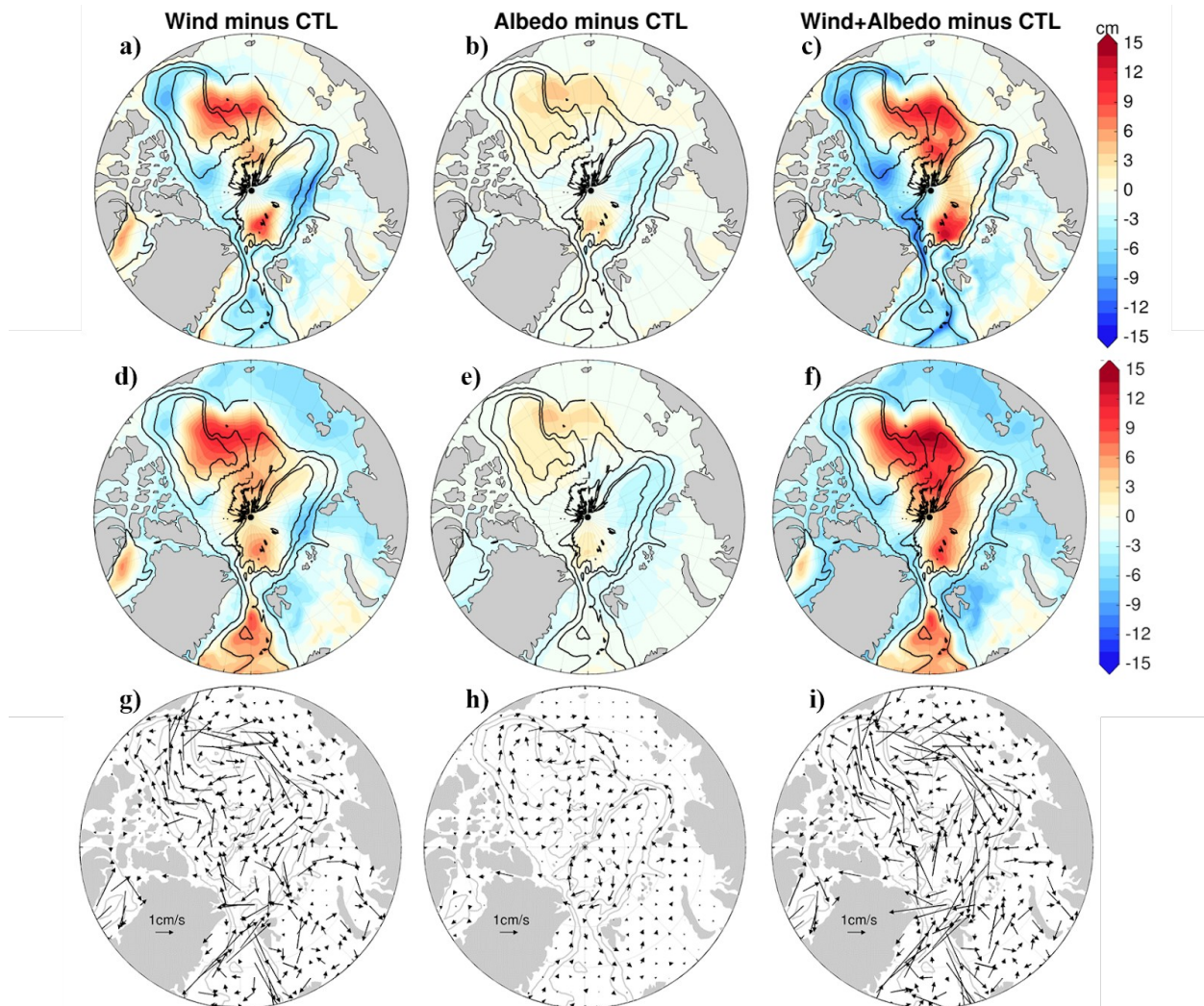
259

The differences in surface stress lead to differences in Ekman transport. In the  
 260 experiments with replaced wind forcing the general transport pattern in the central Arctic is from  
 261 the Canadian Basin towards the Eurasian side. In the Nordic Seas, the difference in Ekman  
 262 transport is directed towards Fram Strait and the Barents Sea Opening and in the northern  
 263 Barents Sea the difference in transport is directed towards the central Arctic (Figure 6d,f). The  
 264 differences in Ekman transport in the albedo experiment are relatively small, and directed from  
 265 Eurasian Basin toward the central Arctic. North of Fram Strait there is a small area with Ekman  
 266 convergence (Figure 6e).

267

In the Arctic, the differences in Ekman transports lead to a redistribution of low salinity  
 268 ocean surface water. Regions of freshwater convergence (divergence) driven by Ekman transport  
 269 show an increase (decrease) in halosteric height (Figure 7a-c). Two regions with increased steric  
 270 height emerge for both the wind replacement experiment and the albedo reduction experiment: In  
 271 the Canadian Basin freshwater is shifted from the boundaries towards the center and in the  
 272 Eurasian Basin increased heightened steric height is visible north of Fram Strait, while a  
 273 decrease is visible north of the Barents and Kara Seas and in the Nordic Seas. The differences in

274 steric height are overall smaller for the albedo case but the effect of sea ice reduction amplifies  
 275 the effect of wind perturbation in the third sensitivity experiment, where both perturbations were  
 276 applied.



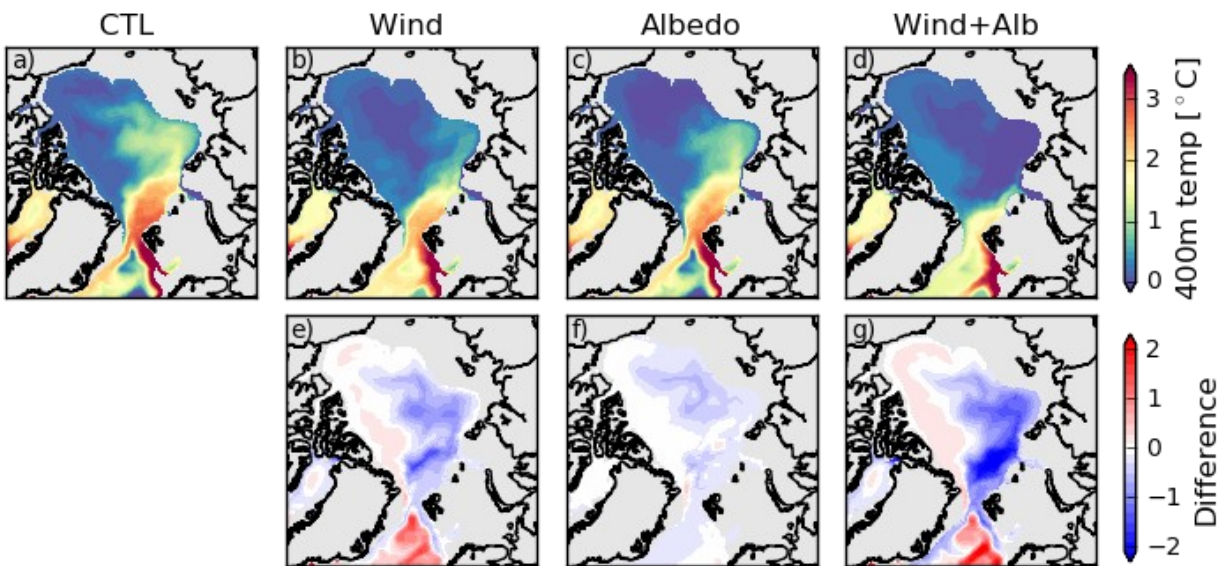
277  
 278 **Figure 7.** Halosteric height difference [cm] (a-c), sea surface height difference [cm] (d-f) and difference in  
 279 geostrophic surface current velocity [cm/s] (g-i) for the three sensitivity experiments compared to the control  
 280 simulation.

281 The differences in total sea surface height between the sensitivity runs and the control run  
 282 are shown in Figure 7d-f. While these changes are driven by freshwater distribution changes in  
 283 the Arctic basin, this is not the case for the Nordic Seas, where increased sea surface height in  
 284 the experiments WIND and WIND+ALB cannot be explained by salinity changes and is  
 285 accompanied by warmer temperatures.

286 The differences in sea surface height lead to differences in surface geostrophic velocity.  
 287 In the WIND experiment the velocity anomaly is anticyclonic over the Arctic basin and south of

288 Fram Strait, in the Nordic Seas the velocity anomaly is anticyclonic as well (Figure 7g). Just  
 289 north of Fram Strait the difference in geostrophic surface current points westward. In the  
 290 ALBEDO experiment, there is also an anticyclonic surface geostrophic current anomaly, mostly  
 291 confined to the Canadian Basin (Figure 7h). In the Eurasian Basin, there is a weak cyclonic  
 292 anomaly in surface geostrophic velocity. The effect of the wind replacement is amplified again  
 293 by sea ice decline in the experiment where wind and albedo are considered together (Figure 7i).

294 Finally, the effect of applying the wind from the coupled model and reducing sea ice  
 295 cover on the horizontal temperature distribution at 400 m depth is evaluated (Figure 8).  
 296 Compared to the control run, applying the wind from the coupled model leads to colder  
 297 temperatures north of Fram Strait and along the cyclonic boundary current pathway. Warmer  
 298 temperature can be seen along the Greenland and Canadian slope and in the Greenland Sea  
 299 (Figure 8e).



300

301 **Figure 8.** Mean temperature [°C] and temperature differences to control simulation [°C] at 400 m depth.

302

303

304

305

306

307

308

309

In experiment ALBEDO a slight cold bias has developed along the deep boundary  
 current pathway, most pronounced at the intersection of the Eurasian Basin, the Lomonosov  
 Ridge and the Canadian Basin, and in the Greenland Sea (Figure 8f). When wind replacement  
 and albedo reduction are combined, the cold biases get larger (Figure 8g); in fact the warm AW  
 is no longer visible in the boundary current beyond the Barents Sea (Figure 8d). Instead, a cold  
 pool in the Eurasian Basin and warmer temperatures north of Greenland and Canadian Arctic  
 Archipelago and along the southern boundary of the Canadian Basin imply a reversal of the AW  
 flow to be anticyclonic (Figure 8d). The biased temperature distribution is remarkably similar to

310 the one in the coupled set-up (Figure 2b), thereby increasing confidence that biases in the  
 311 coupled system can be explained by analyzing the sensitivity experiments in an ocean-only  
 312 configuration.

#### 313 **4 Discussion**

314 The sensitivity experiments performed with the forced ocean-sea ice model show that a  
 315 bias in surface pressure and wind field over the Arctic, like the one present in AWI-CM1,  
 316 together with an underestimation of the sea ice cover can result in an unrealistic temperature  
 317 distribution at 400 m depth. In this case, the warm AW is no longer visible in the boundary  
 318 current beyond the Barents Sea; instead a cold pool emerges in the eastern Eurasian Basin. At the  
 319 same time warmer temperatures appear along the western boundary of the Arctic Ocean and in  
 320 the Greenland Sea south of Fram Strait. These changes imply that part of the AW that does enter  
 321 the Arctic Ocean is directed westwards and circulates the Canadian Basin anticyclonically; they  
 322 also imply that less of the warm AW propagates from the Nordic Seas into the Arctic Ocean.

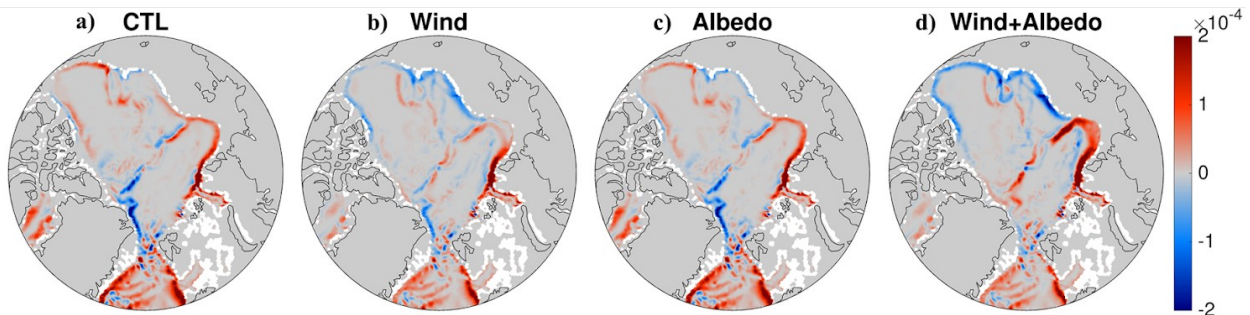
323 To investigate the former point, we computed the depth-average topostrophy between  
 324 300 m and 3,000 m. The concept of topostrophy was introduced by Holloway et al. (2007) as  
 325 part of the Arctic Ocean Model Intercomparison Project (AOMIP, Proshutinsky et al. (2001)) in  
 326 order to compare the simulated circulation between models. The velocity vector field is reduced  
 327 to a scalar quantity  $\tau$  that characterizes the tendency of a current to follow topographic slopes:

$$328 \quad \tau = (\mathbf{V} \times \nabla D) \cdot \mathbf{z},$$

329 where  $\mathbf{V}$  is velocity,  $D$  is the depth gradient, and  $\mathbf{z}$  is the unit vertical vector. A positive value  
 330 indicates a current with shallower water to the right (northern hemisphere) – in the case of the  
 331 Arctic Circumpolar Boundary Current (ACBC) positive topostrophy indicates a cyclonic flow  
 332 direction. The control simulation shows a mostly cyclonic flow all around the Arctic Ocean  
 333 Basin, except for a small area north of Greenland (Figure 9a). With wind forcing from the  
 334 coupled model, the circulation in the Canadian Basin turns anticyclonic (Figure 9b), most  
 335 prominently on the East Siberian side. In the ALBEDO experiment the sense of the circulation  
 336 over continental slopes is barely affected, only the current north of the East Siberian Sea has a  
 337 slightly higher anticyclonic tendency (Figure 9c). In the experiment WIND+ALB, the circulation  
 338 in most of the Canadian Basin is clearly anticyclonic, while the cyclonic circulation in the  
 339 Eurasian Basin seems strengthened (Figure 9d).

340 In the experiments with the replaced wind forcing the mean net volume transport through  
 341 the Barents Sea Opening is higher in the experiments WIND (2.4 Sv) and WIND+ALB (2.7 Sv)  
 342 than for CTL (2.1 Sv) and ALB (2.3 Sv). These changes are associated with the reduced SSH in  
 343 the northern Barents Sea (Figure 7). The AW loses most of its heat in the Barents Sea region  
 344 before entering the Arctic deep basin (Smedsrud et al. 2013) so the increased AW transport  
 345 through the BSO strengthens the anticyclonic boundary circulation in the eastern Eurasian Basin  
 346 (Figure 9), but it rather feeds more cold water there (Figure 8d). This effect is the most  
 347 prominent in the WIND+ALB experiment which has the strongest increase in BSO inflow.

348 Looking at the Nordic Seas, in both simulations with replaced wind forcing the West  
 349 Spitsbergen Current (WSC) and the East Greenland Current (EGC) have weakened compared to  
 350 the control simulation.

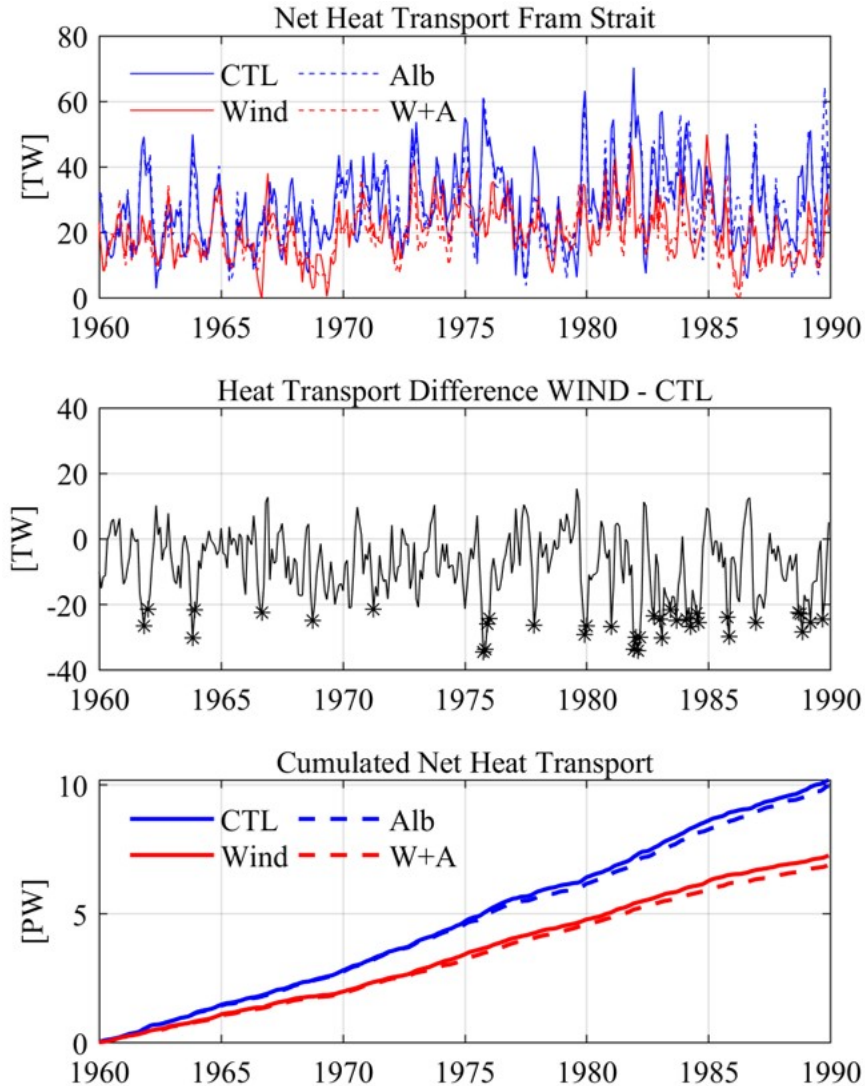


351

352 **Figure 9.** Mean topography below 280 m depth [ $\text{m}^2/\text{s}$ ] for the control simulation (CTL) and three sensitivity  
 353 experiments: Wind, Albedo and Wind+Albedo.  
 354

355 Next, we looked at volume (not shown) and heat transports through Fram Strait at a  
 356 section at  $79^\circ\text{N}$ . The mean monthly net flow of heat through Fram Strait into the Arctic is higher  
 357 for the control simulation (28.3 TW) and experiment ALBEDO (27.7 TW) than for the  
 358 experiments WIND (20.2 TW) and WIND+ALB (19.1 TW) (Figure 10 a). Accumulated over 32  
 359 years of simulation, the net heat transport into the Arctic is 29% less in the WIND experiment  
 360 and 32% less in the experiment WIND+ALB (Figure 10 c).

361

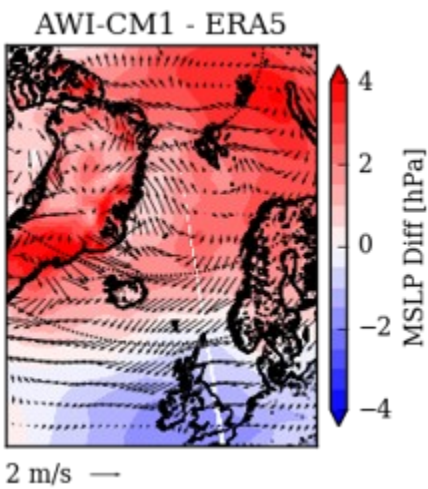


362

363 **Figure 10.** Time series of monthly net heat transport [TW] through Fram Strait for all experiments (a), difference  
 364 [TW] between experiment ‘Wind’ and ‘CTL’; months below 10th percentile are marked with stars (b), cumulated  
 365 net heat transport [TW] for all experiments (c).  
 366

367 The monthly difference in net heat transport into the Arctic between experiment WIND  
 368 and CTL is shown in Figure 10b. The monthly net heat transport through Fram Strait in the  
 369 control simulation is larger most of the time. This can be explained by the wind bias over the  
 370 Nordic Seas (Figure 11). Chatterjee et al. (2018) investigated the impact of the Greenland Sea  
 371 Gyre (GSG) circulation on AW temperature variability at Fram Strait based on ocean reanalysis  
 372 data and found that cold anomalies at Fram Strait are related to an atmospheric pattern that  
 373 shows a high pressure anomaly centered over Svalbard, northerly winds over the western  
 374 Greenland Sea and southerly wind along the Norwegian coast (Chatterjee et al. 2018, see their

375 figure 3c). Such a wind pattern, which resembles the model bias in AWI-CM1, leads to Ekman  
 376 convergence in the GSG and positive sea surface height anomalies which weaken the cyclonic  
 377 GSG circulation. Figure 7d shows the difference in SSH between the ‘Wind’ experiment and the  
 378 control run with a positive height difference in the Nordic Seas. A composite of sea surface  
 379 height differences in the months with the largest negative net heat transport differences (Figure  
 380 10b, starred months show 10<sup>th</sup> percentile) shows even higher SSH differences (not shown). The  
 381 increased SSH in the Nordic Seas reduces AW transport to the Nordic Seas across Iceland-  
 382 Scotland Ridge (not shown). Therefore, the wind anomaly both reduces AW transport toward the  
 383 Arctic Ocean and increases the amount of AW leaving through the BSO. The consequence is the  
 384 reduction in the AW transport in the West Spitsbergen Current at Fram Strait and in the AW  
 385 recirculation in the EGC.  
 386



387  
 388 **Figure 11.** AWI-CM1 MSLP [hPa] and wind bias compared to ERA5 with focus on the Nordic Seas  
 389

390 Because we set out to understand the influence of large-scale wind biases in a coupled  
 391 model, we did not separate the wind bias into a local (over the central Arctic) and remote (over  
 392 the Nordic Seas) component for the sensitivity experiments. Nonetheless, the results discussed  
 393 above are consistent with previous model studies on the role of local and remote wind forcing for  
 394 the ACBC: Lique et al. (2015) and Lique and Johnson (2015) studied the influence of local and  
 395 remote wind forcing on the AW circulation at depth. They found that remote wind forcing over  
 396 the Nordic and Barents Seas can drive a direct and fast response of the AW circulation in the  
 397 Arctic Ocean through a change of AW inflow, while the local wind forcing of the Canadian

398 Basin results in slower changes ‘filtered’ by the surface circulation which in turn modulates the  
399 deeper AW circulation. Here, a stronger anticyclonic wind forces a strong, deep Beaufort Gyre in  
400 the same direction, so that no deep counterflow can develop.

401         Although the bias in sea ice cover does not affect net heat transports through Fram Strait  
402 (Figure 10c), the sensitivity experiment with reduced albedo shows that a reduced sea ice cover  
403 does influence the distribution of freshwater at the surface (Figure 7b). Its effect on the ocean  
404 surface is smaller compared to the wind bias but it also leads to a strengthening of the  
405 anticyclonic surface current in the western Arctic (Figure 7h). This effect of sea ice decline on  
406 the surface dynamics of the Arctic Ocean was also shown by Wang et al. (2019). (2019). Earlier,  
407 Spall (2013) had shown, based on idealized model simulations, that when the ice-ocean stress  
408 was removed completely, the anticyclonic circulation in the western basin is lost and eddy fluxes  
409 from the boundary are enhanced, indicating that the instability of the boundary current is  
410 suppressed by ice cover. Ideally, this potential consequence of sea ice decline and related  
411 feedback should be further investigated with skillful coupled models projecting future Arctic  
412 conditions.

413

414         This study has investigated the influence of a SLP and wind bias specific to the coupled  
415 climate model AWI-CM1. It is worth stressing that this bias is not unique to AWI-CM1 –  
416 another CMIP6 model, MPI-ESM, that also employs ECHAM6.3 as its atmosphere component  
417 but has a different ocean-sea ice component, shows a nearly identical SLP bias, both in shape  
418 and magnitude. Furthermore, it has been found in other atmospheric models as well and it is the  
419 prominent feature in multi-model-means of SLP bias in model intercomparison studies of  
420 coupled and uncoupled models (Walsh et al. 2002). The truncation of the North Atlantic storm  
421 track, which prevents Atlantic cyclones from moving further north into the Norwegian, Barents  
422 and Kara Seas region in the models, has been suggested as a cause for this bias. It has also been  
423 suggested that biased surface winds in the Arctic can adversely affect sea ice transport and the  
424 resulting distribution of sea ice concentration and thickness, as well as the export of ice and  
425 freshwater to the North Atlantic (Walsh et al. 2002; Chapman and Walsh 2007). Our study  
426 shows that this wind bias pattern can additionally affect the simulated circulation in the deep  
427 Arctic Ocean by imposing an anticyclonic surface circulation anomaly which in turn imprints on

428 the deeper ocean circulation. Our results also reveal that a negative sea ice bias could amplify  
429 this issue.

430 Walsh et al. (2002) recommended that efforts to ameliorate the SLP bias in atmospheric  
431 models should be focused on the representation of topography over northern Asia and Greenland  
432 and specifically topographic parameterizations which could affect the exchange of mass between  
433 Asia and the Arctic Ocean. They note that the resolution of the atmosphere model may also play  
434 a role for the magnitude of the bias. For AWI-CM1, we tried tuning some parameters related to  
435 model topography (*gk\_wake*, *gk\_drag* and *gk\_lift*) without being able to significantly reduce the  
436 SLP bias or the circulation bias (not shown).

437 Mu et al. (2020) showed that the assimilation of sea surface temperature into AWI-CM1  
438 leads to a more realistic atmospheric circulation and did reverse the erroneous direction of the  
439 deep boundary current carrying AW after 8 simulation years with data assimilation. This reversal  
440 of the current to a cyclonic flow is attributed to the improvement of atmosphere states over the  
441 ice-free area that can further propagate to the whole Arctic dynamically.

## 442 **5 Conclusions**

443 Atlantification might be an important driver in amplified Arctic sea ice melting and  
444 warming (Årthun et al. 2019) and regional differences in sea ice loss (Årthun et al. 2021). In  
445 order to study the evolution of Atlantification and the associated feedback in the Arctic climate  
446 system with global coupled climate models, the AW inflow and Arctic Ocean circulation need to  
447 be simulated realistically. A skill assessment of the AW layer representation in CMIP5 (Shu et  
448 al. 2019) and CMIP6 (Khosravi et al., submitted) models show that in many of the models that  
449 do simulate a distinct Arctic AW layer, this layer is too thick, too deep or does not show the  
450 observed warming trend. These types of biases are commonly related to insufficient resolution  
451 and too much mixing in the ocean component as well as unrealistic Atlantik-Arctic Ocean  
452 exchange.

453 Our study shows that even if all impediments for simulating AW realistically are addressed in  
454 the ocean model, e.g. sufficient resolution in the horizontal and vertical, Arctic gateways-  
455 resolving grid resolution and bathymetry, the right amount of mixing, etc., new obstacles may  
456 arise after coupling to an atmosphere model with its own shortcomings in the Arctic. AWI-CM1,  
457 like many other coupled climate models, has a bias in SLP over the Arctic Ocean with higher

458 pressure over the Eurasian Basin and Barents and Kara Seas and lower SLP over the Canada  
459 Basin. In the Arctic Ocean, the bias in wind stress related to the biased surface pressure gradient  
460 leads to differences in Ekman transport, freshwater distribution and steric height that strengthens  
461 the anticyclonic surface circulation in the Canadian Basin, so that the deep counterflow gets  
462 reversed. This effect is visualized by negative topostrophy (Figure 9b,d) and the warm bias  
463 (Figure 8e,g) in the Canada Basin. An underestimation of sea ice concentration as seen in AWI-  
464 CM1 can amplify the described processes locally. In the Nordic Seas, an anticyclonic wind bias  
465 increases the sea surface height and weakens the cyclonic gyre circulation there, which leads to  
466 reduced volume and heat (proxy for AW) transport into the Arctic Ocean through Fram Strait. At  
467 the same time, the wind bias also increases AW transport through the BSO, which feeds cold  
468 water to the deep basin. The overall effect is a cold bias in the Eurasian Basin (Figure 8e,g).

469 The problem of biased SLP over the Arctic cannot be overcome easily. Efforts to tune  
470 parameters related to model topography as suggested by Walsh et al. (2002) did not lead to a  
471 significant reduction of the SLP bias or the circulation bias in our practice. SST assimilation  
472 seems to rectify the circulation in AWI-CM1, but this constraint cannot be applied to the future  
473 scenario simulations of course.

474 Currently, a new version 3 of AWI-CM is in development. In this version, ECHAM is  
475 replaced with open IFS (OFIS, Roberts et al. (2018)) for the atmosphere component. Preliminary  
476 results show that the SLP bias over the Arctic is also present in OFIS but it is of smaller  
477 magnitude than in ECHAM. The temperature distribution at 400 m implies a cyclonic  
478 circumpolar circulation in simulations with AWI-CM3. This new model version is not released  
479 yet, and will be described later separately after the initial model tuning process is finished.

480 The Arctic is a hotspot in global warming, but there is still a large inter-model spread and  
481 model uncertainty in CMIP6 projections of the surface warming - especially in the Arctic (Cai et  
482 al. 2021). Detailed investigations of model biases are needed to improve the simulations and  
483 reduce sources of model uncertainty. Simulating ocean heat transport into and within the Arctic  
484 more faithfully will help to understand and predict future Arctic changes better.

## 485 **Acknowledgments and Data Availability**

486 C. Hinrichs, T. Semmler, and T. Jung have received funding from the European Union's  
487 Horizon 2020 Research and Innovation program through grant agreement No. 727862

488 APPLICATE. This is a contribution to the Year of Polar Prediction (YOPP), a flagship activity  
 489 of the Polar Prediction Project (PPP), initiated by the World Weather Research Programme  
 490 (WWRP) of the World Meteorological Organisation (WMO). We acknowledge the WMO  
 491 WWRP for its role in coordinating this international research activity. The work described in this  
 492 paper has also received funding from the Helmholtz Association through the project ‘Regional  
 493 Climate Change (REKLIM)’ and “Advanced Earth System Model Capacity”. The simulations  
 494 were performed at the German Climate Computing Center (DKRZ) using ESM-Tools  
 495 (<https://www.esm-tools.net/>).

496 Our model simulations were compared to the Polar science center Hydrographic  
 497 Climatology (PHC) version 3.0 (available at [http://psc.apl.washington.edu/nonwp\\_projects/PHC/](http://psc.apl.washington.edu/nonwp_projects/PHC/Climatology.html)  
 498 [Climatology.html](http://psc.apl.washington.edu/nonwp_projects/PHC/Climatology.html)), to ERA5 reanalysis data (downloaded from the Copernicus data store at  
 499 <https://cds.climate.copernicus.eu/cdsapp#!/home>), and sea ice concentration data from the  
 500 National Snow & Ice Data Center (<https://nsidc.org/>).

501 Data from the sensitivity experiments will be made available at <https://zenodo.org/> for  
 502 before final submission.

## 503 **References**

504

- 505 Aagaard, K. 1989. *A synthesis of the Arctic Ocean circulation*. Le Conseil.
- 506 Årthun, M., T. Eldevik, and L.H. Smedsrud. 2019. The role of Atlantic heat transport in future Arctic winter sea ice  
 507 loss. *Journal of Climate* 32: 3327-3341.
- 508 Årthun, M., I.H. Onarheim, J. Dörr, and T. Eldevik. 2021. The Seasonal and Regional Transition to an Ice-Free  
 509 Arctic. *Geophysical Research Letters* 48: e2020GL090825.
- 510 Barton, B.I., Y.-D. Lenn, and C. Lique. 2018. Observed Atlantification of the Barents Sea causes the polar front to  
 511 limit the expansion of winter sea ice. *Journal of Physical Oceanography* 48: 1849-1866.
- 512 Beszczynska-Möller, A., E. Fahrbach, U. Schauer, and E. Hansen. 2012. Variability in Atlantic water temperature  
 513 and transport at the entrance to the Arctic Ocean, 1997–2010. *ICES Journal of Marine Science* 69: 852-  
 514 863.
- 515 Cai, Z., Q. You, F. Wu, H.W. Chen, D. Chen, and J. Cohen. 2021. Arctic warming revealed by multiple CMIP6  
 516 models: evaluation of historical simulations and quantification of future projection uncertainties. *Journal of*  
 517 *Climate*: 1-52.
- 518 Cavalieri, D.J., C. L. Parkinson, P. Gloersen, and H. J. Zwally. 1996. Sea Ice Concentrations from Nimbus-7 SMMR  
 519 and DMSP SSM/I-SSMIS Passive Microwave Data, Version 1., ed. Colorado USA. NASA National  
 520 Snow and Ice Data Center Distributed Active Archive Center. Boulder.

- 521 Chapman, W.L., and J.E. Walsh. 2007. Simulations of Arctic temperature and pressure by global coupled models.  
522 *Journal of Climate* 20: 609-632.
- 523 Charnock, H. 1955. Wind stress on a water surface. *Quarterly Journal of the Royal Meteorological Society* 81: 639-  
524 640.
- 525 Chatterjee, S., R.P. Raj, L. Bertino, Ø. Skagseth, M. Ravichandran, and O.M. Johannessen. 2018. Role of Greenland  
526 Sea Gyre Circulation on Atlantic Water Temperature Variability in the Fram Strait. *Geophysical Research*  
527 *Letters* 0.
- 528 Cohen, J., X. Zhang, J. Francis, T. Jung, R. Kwok, J. Overland, T. Ballinger, U. Bhatt, H. Chen, and D. Coumou.  
529 2020. Divergent consensus on Arctic amplification influence on midlatitude severe winter weather.  
530 *Nature Climate Change* 10: 20-29.
- 531 Danilov, S., Q. Wang, R. Timmermann, N. Iakovlev, D. Sidorenko, M. Kimmritz, T. Jung, and J. Schröter. 2015.  
532 Finite-Element Sea Ice Model (FESIM), version 2. *Geosci. Model Dev.* 8: 1747-1761.
- 533 Dmitrenko, I.A., I.V. Polyakov, S.A. Kirillov, L.A. Timokhov, I.E. Frolov, V.T. Sokolov, H.L. Simmons, V.V.  
534 Ivanov, and D. Walsh. 2008. Toward a warmer Arctic Ocean: Spreading of the early 21st century Atlantic  
535 Water warm anomaly along the Eurasian Basin margins. *Journal of Geophysical Research: Oceans* 113.
- 536 Golubeva, E., and G. Platov. 2007. On improving the simulation of Atlantic Water circulation in the Arctic Ocean.  
537 *Journal of Geophysical Research: Oceans* 112.
- 538 Good, S.A., M.J. Martin, and N.A. Rayner. 2013. EN4: Quality controlled ocean temperature and salinity profiles  
539 and monthly objective analyses with uncertainty estimates. *Journal of Geophysical Research: Oceans* 118:  
540 6704-6716.
- 541 Griffies, S.M., A. Biastoch, C. Böning, F. Bryan, G. Danabasoglu, E.P. Chassignet, M.H. England et al. 2009.  
542 Coordinated Ocean-ice Reference Experiments (COREs). *Ocean Modelling* 26: 1-46.
- 543 Holloway, G., F. Dupont, E. Golubeva, S. Häkkinen, E. Hunke, M. Jin, M. Karcher, F. Kauker, M. Maltrud, and  
544 M.M. Maqueda. 2007. Water properties and circulation in Arctic Ocean models. *Journal of Geophysical*  
545 *Research: Oceans* 112.
- 546 Holloway, G., and Z. Wang. 2009. Representing eddy stress in an Arctic Ocean model. *Journal of Geophysical*  
547 *Research: Oceans* 114.
- 548 Ilicak, M., H. Drange, Q. Wang, R. Gerdes, Y. Aksenov, D. Bailey, M. Bentsen et al. 2016. An assessment of the  
549 Arctic Ocean in a suite of interannual CORE-II simulations. Part III: Hydrography and fluxes. *Ocean*  
550 *Modelling* 100: 141-161.
- 551 Itkin, P., M. Karcher, and R. Gerdes. 2014. Is weaker Arctic sea ice changing the Atlantic water circulation? *Journal*  
552 *of Geophysical Research: Oceans* 119: 5992-6009.
- 553 Ivanov, V., A. Smirnov, V. Alexeev, N.V. Koldunov, I. Repina, and V. Semenov. 2018. Contribution of  
554 Convection-Induced Heat Flux to Winter Ice Decay in the Western Nansen Basin. *Journal of Geophysical*  
555 *Research: Oceans* 123: 6581-6597.

- 556 Jung, T., N.D. Gordon, P. Bauer, D.H. Bromwich, M. Chevallier, J.J. Day, J. Dawson, F. Doblas-Reyes, C. Fairall,  
557 and H.F. Goessling. 2016. Advancing polar prediction capabilities on daily to seasonal time scales. *Bulletin*  
558 *of the American Meteorological Society* 97: 1631-1647.
- 559 Karcher, M., F. Kauker, R. Gerdes, E. Hunke, and J. Zhang. 2007. On the dynamics of Atlantic Water circulation in  
560 the Arctic Ocean. *Journal of Geophysical Research: Oceans* 112.
- 561 Khosravi, N., Q. Wang, N. Koldunov, C. Hinrichs, T. Semmler, S. Danilov, and T. Jung. Arctic Ocean in CMIP6  
562 Models: Historical and projected temperature and salinity in the deep basins. *Earth's Future*. Preprint  
563 available at <https://www.essoar.org/doi/abs/10.1002/essoar.10505254.1>.
- 564 Koenigk, T., and L. Brodeau. 2014. Ocean heat transport into the Arctic in the twentieth and twenty-first century in  
565 EC-Earth. *Climate Dynamics* 42: 3101-3120.
- 566 Koldunov, N.V., V. Aizinger, N. Rakowsky, P. Scholz, D. Sidorenko, S. Danilov, and T. Jung. 2019. Scalability and  
567 some optimization of the Finite-volume Sea ice–Ocean Model, Version 2.0 (FESOM2). *Geoscientific*  
568 *Model Development* 12: 3991-4012.
- 569 Large, W.G., and S. Yeager. 2009. The global climatology of an interannually varying air–sea flux data set. *Climate*  
570 *Dynamics* 33: 341-364.
- 571 Lique, C., and H.L. Johnson. 2015. Is there any imprint of the wind variability on the Atlantic Water circulation  
572 within the Arctic Basin? *Geophysical Research Letters* 42: 9880-9888.
- 573 Lique, C., H.L. Johnson, and P.E.D. Davis. 2015. On the Interplay between the Circulation in the Surface and the  
574 Intermediate Layers of the Arctic Ocean. *Journal of Physical Oceanography* 45: 1393-1409.
- 575 Maqueda, M.M., and G. Holloway. 2006. Second-order moment advection scheme applied to Arctic Ocean  
576 simulation. *Ocean Modelling* 14: 197-221.
- 577 Mu, L., L. Nerger, Q. Tang, S.N. Loza, D. Sidorenko, Q. Wang, T. Semmler, L. Zampieri, M. Losch, and H.F.  
578 Goessling. 2020. Toward a data assimilation system for seamless sea ice prediction based on the AWI  
579 climate model. *Journal of Advances in Modeling Earth Systems* 12: e2019MS001937.
- 580 Müller, W.A., J.H. Jungclaus, T. Mauritsen, J. Baehr, M. Bittner, R. Budich, F. Bunzel, M. Esch, R. Ghosh, and H.  
581 Haak. 2018. A Higher-resolution Version of the Max Planck Institute Earth System Model (MPI-ESM1.  
582 2-HR). *Journal of Advances in Modeling Earth Systems* 10: 1383-1413.
- 583 Nazarenko, L., G. Holloway, and N. Tausnev. 1998. Dynamics of transport of “Atlantic signature” in the Arctic  
584 Ocean. *Journal of Geophysical Research: Oceans* 103: 31003-31015.
- 585 Polyakov, I.V., A. Beszczynska, E.C. Carmack, I.A. Dmitrenko, E. Fahrbach, I.E. Frolov, R. Gerdes, E. Hansen, J.  
586 Holfort, and V.V. Ivanov. 2005. One more step toward a warmer Arctic. *Geophysical Research Letters* 32.
- 587 Polyakov, I.V., U.S. Bhatt, J.E. Walsh, E.P. Abrahamson, A.V. Pnyushkov, and P.F. Wassmann. 2013. Recent  
588 oceanic changes in the Arctic in the context of long-term observations. *Ecological Applications* 23: 1745-  
589 1764.
- 590 Polyakov, I.V., A.V. Pnyushkov, M.B. Alkire, I.M. Ashik, T.M. Baumann, E.C. Carmack, I. Goszczko, J. Guthrie,  
591 V.V. Ivanov, and T. Kanzow. 2017. Greater role for Atlantic inflows on sea-ice loss in the Eurasian Basin  
592 of the Arctic Ocean. *Science* 356: 285-291.

- 593 Polyakov, I.V., T.P. Rippeth, I. Fer, M.B. Alkire, T.M. Baumann, E.C. Carmack, R. Ingvaldsen et al. 2020.  
594 Weakening of Cold Halocline Layer Exposes Sea Ice to Oceanic Heat in the Eastern Arctic Ocean. *Journal*  
595 *of Climate* 33: 8107-8123.
- 596 Proshutinsky, A., M. Steele, J. Zhang, G. Holloway, N. Steiner, S. Häkkinen, D. Holland, R. Gerdes, C. Köberle,  
597 and M. Karcher. 2001. The Arctic Ocean Model Intercomparison Project (AOMIP). *Eos Trans. AGU* 82:  
598 637-644.
- 599 Rackow, T., H.F. Goessling, T. Jung, D. Sidorenko, T. Semmler, D. Barbi, and D. Handorf. 2016. Towards multi-  
600 resolution global climate modeling with ECHAM6-FESOM. Part II: climate variability. *Climate Dynamics*:  
601 1-26.
- 602 Roberts, C.D., R. Senan, F. Molteni, S. Boussetta, M. Mayer, and S.P. Keeley. 2018. Climate model configurations  
603 of the ECMWF Integrated Forecasting System (ECMWF-IFS cycle 43r1) for HighResMIP. *Geoscientific*  
604 *Model Development* 11: 3681-3712.
- 605 Rudels, B., H.J. Friedrich, and D. Quadfasel. 1999. The Arctic circumpolar boundary current. *Deep Sea Research*  
606 *Part II: Topical Studies in Oceanography* 46: 1023-1062.
- 607 Semmler, T., S. Danilov, P. Gierz, H.F. Goessling, J. Hegewald, C. Hinrichs, N. Koldunov et al. 2020. Simulations  
608 for CMIP6 With the AWI Climate Model AWI-CM-1-1. *Journal of Advances in Modeling Earth Systems*  
609 12: e2019MS002009.
- 610 Serreze, M., A. Barrett, J. Stroeve, D. Kindig, and M. Holland. 2009. The emergence of surface-based Arctic  
611 amplification. *The Cryosphere* 3: 11.
- 612 Serreze, M.C., and R.G. Barry. 2011. Processes and impacts of Arctic amplification: A research synthesis. *Global*  
613 *and planetary change* 77: 85-96.
- 614 Shu, Q., Q. Wang, J. Su, X. Li, and F. Qiao. 2019. Assessment of the Atlantic water layer in the Arctic Ocean in  
615 CMIP5 climate models. *Climate Dynamics* 53: 5279-5291.
- 616 Sidorenko, D., T. Rackow, T. Jung, T. Semmler, D. Barbi, S. Danilov, K. Dethloff, W. Dorn, K. Fieg, and H.F.  
617 Göbbling. 2015. Towards multi-resolution global climate modeling with ECHAM6-FESOM. Part I: model  
618 formulation and mean climate. *Climate Dynamics* 44: 757-780.
- 619 Smedsrud, L.H., I. Esau, R.B. Ingvaldsen, T. Eldevik, P.M. Haugan, C. Li, V.S. Lien, A. Olsen, A.M. Omar, and  
620 O.H. Otterå. 2013. The role of the Barents Sea in the Arctic climate system. *Reviews of Geophysics* 51:  
621 415-449.
- 622 Spall, M.A. 2013. On the Circulation of Atlantic Water in the Arctic Ocean. *Journal of Physical Oceanography* 43:  
623 2352-2371.
- 624 Steele, M., R. Morley, and W. Ermold. 2001. PHC: A global ocean hydrography with a high-quality Arctic Ocean.  
625 *Journal of Climate* 14: 2079-2087.
- 626 Stevens, B., M. Giorgetta, M. Esch, T. Mauritsen, T. Crueger, S. Rast, M. Salzmann, H. Schmidt, J. Bader, and K.  
627 Block. 2013. Atmospheric component of the MPI-M Earth System Model: ECHAM6. *Journal of Advances*  
628 *in Modeling Earth Systems* 5: 146-172.

- 629 Timmermans, M.-L., and J. Marshall. 2020. Understanding Arctic Ocean Circulation: A Review of Ocean Dynamics  
630 in a Changing Climate. *Journal of Geophysical Research: Oceans* 125: e2018JC014378.
- 631 Vihma, T. 2014. Effects of Arctic Sea Ice Decline on Weather and Climate: A Review. *Surveys in Geophysics* 35:  
632 1175-1214.
- 633 Wallace, J.M., I.M. Held, D.W. Thompson, K.E. Trenberth, and J.E. Walsh. 2014. Global warming and winter  
634 weather. *Science* 343: 729-730.
- 635 Walsh, J.E., V.M. Kattsov, W.L. Chapman, V. Govorkova, and T. Pavlova. 2002. Comparison of Arctic climate  
636 simulations by uncoupled and coupled global models. *Journal of Climate* 15: 1429-1446.
- 637 Wang, Q., S. Danilov, D. Sidorenko, R. Timmermann, C. Wekerle, X. Wang, T. Jung, and J. Schröter. 2014. The  
638 Finite Element Sea Ice-Ocean Model (FESOM) v. 1.4: formulation of an ocean general circulation model.  
639 *Geoscientific Model Development* 7: 663-693.
- 640 Wang, Q., M. Ilicak, R. Gerdes, H. Drange, Y. Aksenov, D.A. Bailey, M. Bentsen et al. 2016a. An assessment of the  
641 Arctic Ocean in a suite of interannual CORE-II simulations. Part I: Sea ice and solid freshwater. *Ocean*  
642 *Modelling* 99: 110-132.
- 643 Wang, Q., M. Ilicak, R. Gerdes, H. Drange, Y. Aksenov, D.A. Bailey, M. Bentsen et al. 2016b. An assessment of  
644 the Arctic Ocean in a suite of interannual CORE-II simulations. Part II: Liquid freshwater. *Ocean*  
645 *Modelling* 99: 86-109.
- 646 Wang, Q., C. Wekerle, S. Danilov, D. Sidorenko, N. Koldunov, D. Sein, B. Rabe, and T. Jung. 2019. Recent Sea Ice  
647 Decline Did Not Significantly Increase the Total Liquid Freshwater Content of the Arctic Ocean. *Journal*  
648 *of Climate* 32: 15-32.
- 649 Wang, Q., C. Wekerle, S. Danilov, X. Wang, and T. Jung. 2018. A 4.5 km resolution Arctic Ocean simulation with  
650 the global multi-resolution model FESOM 1.4. *Geoscientific Model Development* 11: 1229.
- 651 Wang, Q., C. Wekerle, X. Wang, S. Danilov, N. Koldunov, D. Sein, D. Sidorenko, W.J. von Appen, and T. Jung.  
652 2020. Intensification of the Atlantic Water supply to the Arctic Ocean through Fram Strait induced by  
653 Arctic sea ice decline. *Geophysical Research Letters* 47: e2019GL086682.
- 654 Woodgate, R.A., K. Aagaard, R.D. Muench, J. Gunn, G. Björk, B. Rudels, A. Roach, and U. Schauer. 2001. The  
655 Arctic Ocean boundary current along the Eurasian slope and the adjacent Lomonosov Ridge: Water mass  
656 properties, transports and transformations from moored instruments. *Deep Sea Research Part I:*  
657 *Oceanographic Research Papers* 48: 1757-1792.
- 658 Zhang, J., and M. Steele. 2007. Effect of vertical mixing on the Atlantic Water layer circulation in the Arctic Ocean.  
659 *Journal of Geophysical Research: Oceans* 112.